IEEE Access
Multidisciplinary ⋮ Rapid Review ⋮ Open Access Journal

Received 6 November 2022, accepted 18 November 2022, date of publication 24 November 2022,
date of current version 1 December 2022.

Digital Object Identifier 10.1109/ACCESS.2022.3224464

RESEARCH ARTICLE

Material Relative Permittivity Determination From the Inhomogeneous Transmission-Line Secondary Parameters

FRANCK MOUKANDA MBANGO[1,2], GHISLAIN FRAIDY BOUESSE[2,3], AND FABIEN NDAGIJIMANA[4]

[1]Faculty of Sciences and Techniques, Marien Ngouabi University, Brazzaville, Congo
[2]Electrical and Electronics Engineering Laboratory, Marien Ngouabi University, Brazzaville, Congo
[3]National School of Polytechnic Studies, Marien Ngouabi University, Brazzaville, Congo
[4]Department of Electrical Engineering, Univ. Grenoble Alpes, CNRS, Grenoble INP, G2ELab, F-38400 Saint-Martin d'Hères, France

Corresponding author: Franck Moukanda Mbango (franck.moukandambango@umng.cg)

ABSTRACT After further transmission line technique investigation, we propose a new approach to material characterization based on the combination of the propagation constant and the characteristic impedance of the transmission-line. Three main elements constitute the approach novelty's root: the determination of the propagation constant without using the eigenvalue principle, the improved mathematical expression of the characteristic impedance, and the automatically corrected coefficient. The two-line technique is based on three required measures, where the most extended fixture is partially filled with the specimen to be tested. As a result, the discontinuities caused by the geometric change of access interfaces and the waveguide dimensions have been solved. The characteristic impedance is determined straight and amended by a third polynomial function degree. The polynomial function and the amended correction coefficient determination are the facilitation parameters of the new approach technique. This new method allows the extraction of the material's complex relative permittivity. The procedure has been validated with the Rogers RO4003C, Alumina 99.6%, and Vinifera (based on the dielectric materials available in our laboratory) through the microstrip fixture in the scanned frequency (0.08–8) GHz by extracting its electric intrinsic parameters. The dielectric constants range from 1.1–10.4, where the thicknesses are 1.54 mm, 2.067 mm, and 1.078 mm have been used. Two identical microstrip test cells with the same geometric dimensions but various lengths have been manufactured. That promotes the feasibility of two measures simultaneously.

INDEX TERMS Characteristic impedance, discontinuity, material intrinsic parameters, propagation constant, semi-full transmission line.

I. INTRODUCTION

Electronic devices are increasingly attractive [1], [2], [3], [4] due to their potential application in several fundamental communication systems: solar cells [5], vehicle communications, satellites, new precision-guided munitions, etc. Understanding the electronic processes in these materials and devices is of fundamental importance to improve electronic performance and develop new materials for future technologies [6], [7]. That justifies the reason for developing advanced characterization techniques [8]. In addition, theoretical models are necessary regarding the properties of electronic materials. The literature suggests several alternative methods in the electromagnetic area [9], [10], [11], classified into two groups: broadband and narrowband [12], destructive and non-destructive [13], [14], [15], resonant and non-resonant [16], [17], direct and indirect methods, or distributed and lumped elements [11]. Inside these two groups are found six main techniques [18], [19], [20] according to the application domain and the state or kind of material to be characterized [21]. These six methods are Free-space [9], [22], [23], resonant cavity [24], [25], [26], capacitive or parallel plates capacitor [27], inductance [11], [28], probes [29], [30], and transmission line [31], [32], [33].

The associate editor coordinating the review of this manuscript and approving it for publication was Wuliang Yin.

Each method has its advantages and drawbacks (disadvantages) that may affect the accuracy of at least one parameter to be measured and the frequency domain to be covered. For example, all material shapes can't be used in the same test cell along with the six techniques. Also, while transmission line (also called waveguide) methods are suitable for broadband measurements, resonator cavity methods provide accurate results for low-loss materials. It means adapting the approach technique to extract parameters, the scanned frequency needed, the kind of material (shape, state, etc.), and the material application domain is essential.

The electronic materials are categorized into three, namely: electric, magnetic and magneto-electric materials. As mentioned above, we need to adapt the method according to the goals to reach. For high or thin wafer thicknesses, the transmission line is well-adapted. The transmission line technique is often used because they offer a good relationship between the accuracy, the scanned frequency, and the material to characterize. The transmission line can present one or two port accesses. The other end of the line can be open [34] or short-circuited [35] for one access. But the technique doesn't help extract the loss tangent.

Recently, a focus on the phase sensibility to extract the dielectric constant has attracted the researchers' attention by using the transmission coefficient through the low-pass filter design frame [36] but didn't cover a wider frequency band. In this paper, we present a technique using two rectangular coaxial identical transmission lines but different lengths ($l_2 \neq l_1$) where the more extended is semi-filled. The developed method uses secondary transmission line parameters: the propagation constant [31], [37], and characteristic impedance combination. This challenge helps the material nature be known: electric, magnetic, or magneto-electric, and scanned a significant range frequency. The extended line is partially-filled up [38], [39], [40]. The two-line technique is famous and one of the best-known throughout the world. The two-line technique procedure utilizes the cascading wave T-matrix (CWM) principle. Such a technique focuses on the length difference via the propagation constant. From that, the new approach has been inspired, and determining the characteristic impedance is a new challenge. It is also proposed in this paper another way to extract the propagation constant instead of using the ideal line eigenvalues. The characteristic impedance mathematical expression has been presented with a particular improvement due to the corrected coefficient determination.

Furthermore, leading corrections at some steps of the method suggest a great view of solving the loss tangent. Finally, the two-line technique through the eigenvalues determination method has validated the new approach through result comparisons to achieve the technique extraction methodology. Therefore, three main points will be presented: the technique bases, experimental results validation, and analysis before a conclusion. The new approach is fundamentally based on the performance of the apparatus

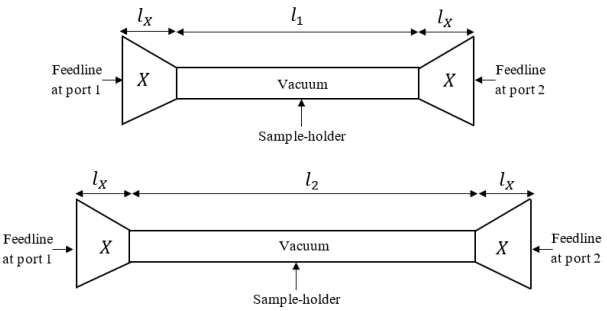

FIGURE 1. Two identical transmission lines with different lengths.

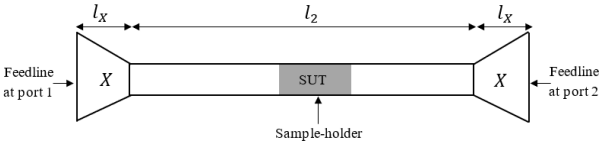

FIGURE 2. A transmission line l_2 partially filled with sample under test (SUT).

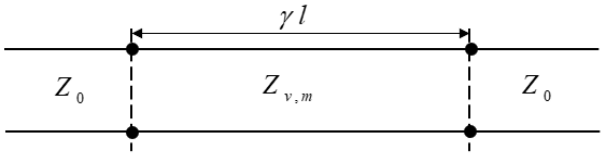

FIGURE 3. A transmission line *l* in the presence of its secondary parameters.

(the sensor) that depends on the contact pressure applied to the sample under test.

II. MATHEMATICAL TECHNIQUE BASIS

Let us consider a two-port transmission line filled up with the vacuum, as illustrated in Fig. 1.

The T-matrixes for both test cells (whose lengths are l_1 and l_2) filled up with the vacuum are defined [32] as follows,

$$[T_1]_v = \frac{1}{S_{21}^{v_1}} \begin{bmatrix} S_{21}^{v_1} S_{12}^{v_1} - S_{11}^{v_1} S_{22}^{v_1} & S_{11}^{v_1} \\ -S_{22}^{v_1} & 1 \end{bmatrix} \quad (1)$$

$$[T_2]_v = \frac{1}{S_{21}^{v_2}} \begin{bmatrix} S_{21}^{v_2} S_{12}^{v_2} - S_{11}^{v_2} S_{22}^{v_2} & S_{11}^{v_2} \\ -S_{22}^{v_2} & 1 \end{bmatrix} \quad (2)$$

and once the specimen to be characterized is partially filled in the extended test cell l_2, as shown in Fig. 2, the transfer matrix becomes as given below,

$$[T_2]_m = \frac{1}{S_{21}^{m_2}} \begin{bmatrix} S_{21}^{m_2} S_{12}^{m_2} - S_{11}^{m_2} S_{22}^{m_2} & S_{11}^{m_2} \\ -S_{22}^{m_2} & 1 \end{bmatrix} \quad (3)$$

According to Figs. 1 and 2, which can be summarized as given in Fig. 3, the equations (1) - (3) can be re-written [41] as,

$$[T_1]_v = \frac{1}{2Z_v Z_0} \times \begin{bmatrix} 2Z_v Z_0 \cosh(\gamma_1 l_1) - A_1 & \left(Z_v^2 - Z_0^2\right) \sinh(\gamma_1 l_1) \\ -\left(Z_v^2 - Z_0^2\right) \sinh(\gamma_1 l_1) & 2Z_v Z_0 \cosh(\gamma_1 l_1) - A_1 \end{bmatrix} \quad (4)$$

For the extended transmission-line, the transfer T-matrix is rewritten as given below,

$$[T_2]_v = \frac{1}{2Z_vZ_0} \times \begin{bmatrix} 2Z_vZ_0\cosh(\gamma_1 l_2) - A_2 & \left(Z_v^2 - Z_0^2\right)\sinh(\gamma_1 l_2) \\ -\left(Z_v^2 - Z_0^2\right)\sinh(\gamma_1 l_2) & 2Z_vZ_0\cosh(\gamma_1 l_2) - A_2 \end{bmatrix} \tag{5}$$

and,

$$[T_2]_m = \frac{1}{2Z_mZ_0} \times \begin{bmatrix} 2Z_mZ_0\cosh(\gamma_2 l_2) - A_3 & \left(Z_m^2 - Z_0^2\right)\sinh(\gamma_2 l_2) \\ -\left(Z_m^2 - Z_0^2\right)\sinh(\gamma_2 l_2) & 2Z_mZ_0\cosh(\gamma_2 l_2) - A_3 \end{bmatrix} \tag{6}$$

where,

$$A_1 = \left(Z_v^2 + Z_0^2\right)\sinh(\gamma_1 l_1)$$
$$A_2 = \left(Z_v^2 + Z_0^2\right)\sinh(\gamma_1 l_2)$$
$$A_3 = \left(Z_m^2 + Z_0^2\right)\sinh(\gamma_2 l_2)$$

Both test cell lengths are linked, as shown in Fig. 2, and expressed in the following equation,

$$l_2 = l_1 + \Delta l \tag{7}$$

The supposed ideal transmission line is Δl long, and the vacuum propagation constant becomes as follows,

$$\gamma_v \Delta l = \gamma_1 (l_2 - l_1) \tag{8}$$

Meanwhile, the propagation constant got in the presence of the material is,

$$\gamma_m \Delta l = \gamma_2 l_2 - \gamma_1 l_l \tag{9}$$

Several studies have been conducted using the two-line techniques [31], [42]. In that case, the resolution of the following equation,

$$[T_{12}]_v = [T_2]_v [T_1]_v^{-1} \tag{10}$$
$$[T_{12}]_m = [T_2]_m [T_1]_v^{-1} \tag{11}$$

where,

$$[T_{12}]_{v,m} = \begin{bmatrix} T^{(1)}_{11_{v,m}} & T^{(2)}_{12_{v,m}} \\ T^{(3)}_{21_{v,m}} & T^{(4)}_{22_{v,m}} \end{bmatrix} \tag{12}$$

establishes a mathematical relation between the transmission line characteristic impedance (Z_v, Z_m) and the impedance access Z_0. The development and calculation give,

$$T^{(2)}_{12_{v,m}} T^{(3)}_{21_{v,m}} = \frac{\left(Z_0^2 - Z_{v,m}^2\right)}{8Z_{v,m}^2 Z_0^2}\left\{1 - \cosh\left(2\gamma_{v,m}\Delta l\right)\right\} \tag{13}$$

The equations (1)-(3) and (10)-(11) through (12) allow the analytical relation between the measured scattering parameters and the material properties to be proposed to solve the problem.

Let us consider that $P_{v,m} = T^{(2)}_{12_{v,m}}.T^{(3)}_{21_{v,m}}$ and $Y_{v,m} = \cosh\left(2\gamma_{v,m}\Delta l\right)$. The resolution of (13) gives four possibilities for results. It's found out that, (14), as shown at the bottom of the page. Or, (15), as shown at the bottom of the page. Simultaneously, the new mathematical formulation through (4)-(6) allows determining the propagation constant as given in (16),

$$\gamma_{v,m}\Delta l = \cosh^{-1}\left(\frac{T^{(1)}_{11_{v,m}} + T^{(4)}_{22_{v,m}}}{2}\right) \tag{16}$$

The literature defines the propagation constant through the Maxwell equation as a combination of the attenuation coefficient αl and the electric length $\beta l = \theta$. In that case,

$$\gamma\,\Delta l = \alpha l + \underbrace{\beta \Delta l}_{\theta} \tag{17}$$

During the procedure, the electric length must be linearized as the phase velocity doesn't depend on the frequency when the transverse electromagnetic (TEM) mode propagates.

An automatic coefficient is determined to correct the characteristic impedance of the fixture when the material under test is inserted. By considering X the correction coefficient, given as shown (18) below,

$$X = \frac{\sum_1^n \theta_m}{\sum_1^n \theta_v} - \frac{\sum_1^n \theta_v}{\sum_1^n \theta_m} \tag{18}$$

both characteristic impedances are (19), as shown at the bottom of the next page, and (20), as shown at the bottom of the next page. The equations (16), (18), (19) and (20) represent the considerable contribution and novelty developed in this paper.

The complex effective permittivity is given in the following equation,

$$\varepsilon^*_{eff} = \frac{\gamma_d}{\gamma_v^c}\frac{Z_v^*}{Z_m^*} \tag{21}$$

$$Z_{v,m} = \pm Z_0\sqrt{\frac{1}{P_{v,m} - 1} + \left\{Y_{v,m} + 2\sqrt{2}\sqrt{2P_{v,m}^2 + \left(1 - Y_{v,m}\right)P_{v,m}} - \left(1 + 4P_{v,m}\right)\right\}} \tag{14}$$

$$Z_{v,m} = \pm Z_0\sqrt{\frac{1}{1 - P_{v,m}} + \left\{-Y_{v,m} + 2\sqrt{2}\sqrt{2P_{v,m}^2 + \left(1 - Y_{v,m}\right)P_{v,m}} + \left(1 + 4P_{v,m}\right)\right\}} \tag{15}$$

where

$$\gamma_d^* = (\alpha_m - \alpha_v)\,\Delta l + j\theta_m \tag{22}$$
$$\gamma_v^c = j\theta_v \tag{23}$$
$$Z_m^* = Z_m' + jZ_m'' \tag{24}$$

and

$$Z_v^* = Z_v' + jZ_v'' \tag{25}$$

When developing (21), it is observed that the real part of that expression has an uncertainty coefficient $\Delta\varepsilon_{eff}'$, changing with the frequency.

$$\Delta\varepsilon_{eff}' = \left\{ \frac{\theta_m Z_v'' Z_m'' + \alpha_d \left(Z_m' Z_v'' - Z_m'' Z_v'\right) \Delta l}{\theta_v \left(Z_m'\right)^2} \right\} \tag{26}$$

In that case, the real part of effective permittivity is about,

$$\varepsilon_{eff}' = \frac{\theta_m}{\theta_v} \frac{Z_a'}{Z_m'} \tag{27}$$

The imaginary part of the equation (21) is below,

$$\varepsilon_{eff}'' = \frac{Z_m' Z_v'' \theta_m - \alpha_m \left(Z_m' Z_v' + Z_m'' Z_v''\right) \Delta l - Z_m'' Z_v' \theta_m}{\theta_v \left(Z_m'\right)^2} \tag{28}$$

This expression highlights two parts: the loss coefficient, as given in (29),

$$\varepsilon_{eff_c}'' = -\frac{\alpha_d \left(Z_m' Z_v' + Z_m'' Z_v''\right) \Delta l}{\theta_v \left(Z_m'\right)^2} \tag{29}$$

and the uncertainty term, as shown,

$$\Delta\varepsilon_{eff}'' = \frac{\left(Z_v'' Z_m' - Z_m'' Z_v'\right) \theta_m}{\theta_v \left(Z_m'\right)^2} \tag{30}$$

with the dielectric attenuation coefficient as follows,

$$\alpha_d = \alpha_m - \alpha_v \tag{31}$$

The effective loss tangent is determined from (27) and (29), as given below,

$$\tan\delta_{eff} = \frac{\alpha_d}{\beta_m} \left(1 + \frac{Z_m'' Z_v''}{Z_v' Z_m'}\right) \tag{32}$$

The equation (32) can also be rewritten as follows,

$$\tan\delta_{eff} = \frac{1}{\beta_v} \left(\frac{\alpha_m}{\sqrt{\varepsilon_{eff}'}} - \alpha_v\right) \left(1 + \frac{Z_m'' Z_v''}{Z_v' Z_m'}\right). \tag{33}$$

III. DIELECTRIC MATERIAL EXTRACTION

Here is described a new method of material characterization when using the inhomogenous fixture, especially the microstrip test cell. From the cell design, as shown in Fig. 4 below,

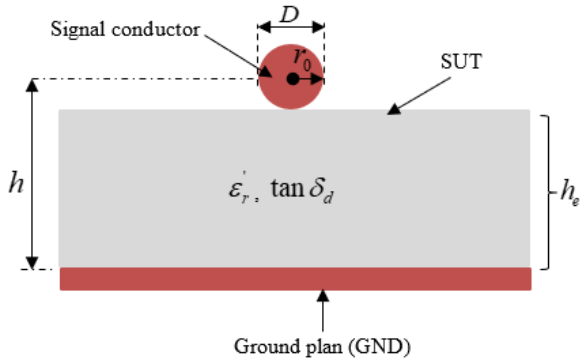

FIGURE 4. A simplified design of the microstrip line having a circular signal conductor.

FIGURE 5. Test cell design is not connected to the VNA without the SUT.

The material thickness is symbolized by h_e while the considered is defined as,

$$h = h_e + \frac{D}{2} \tag{34}$$

The signal conductor is circular with a diameter $D = 2r_0$, where r_0 is its radius. The transition from the effective complex permittivity ε_{eff}^* to the relative complex permittivity ε_r^*

$$Z_v = Z_0 \sqrt{\frac{1}{1 - P_v} + \left\{ -Y_v + 2\sqrt{2} \sqrt{2P_v^2 + (1 - Y_v)\,P_v} + (1 + 4P_v) \right\}} \tag{19}$$

$$Z_m = \frac{Z_0}{X} \sqrt{\frac{1}{P_m - 1} + \left\{ Y_m + 2\sqrt{2} \sqrt{2P_m^2 + (1 - Y_m)\,P_m} - (1 + 4P_m) \right\}} \tag{20}$$

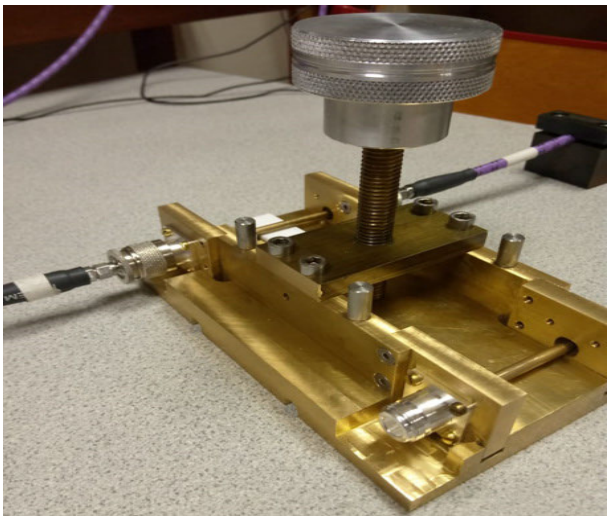

(a)

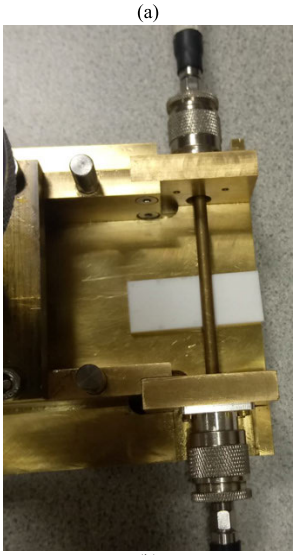

(b)

FIGURE 6. (a) The SUT inside of the microstrip transmission line trapper. (b) Top view of the SUT inside of trapper.

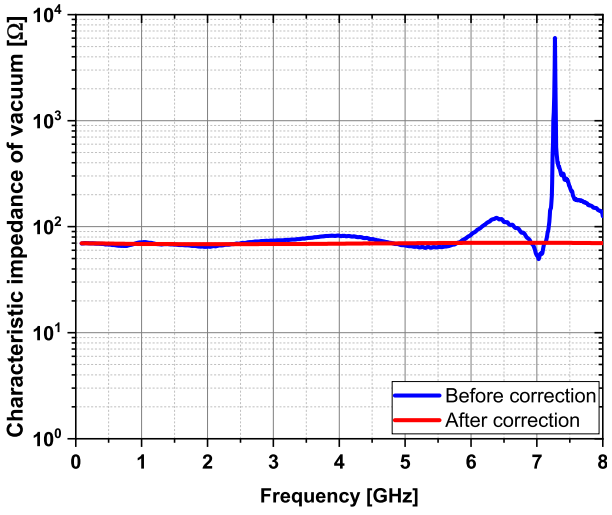

(a)

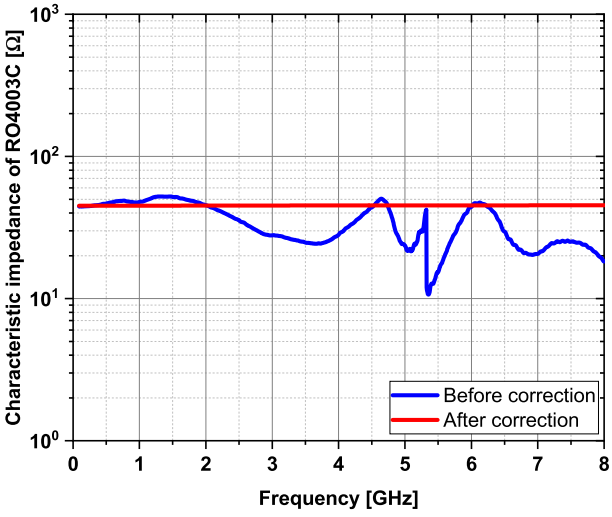

(b)

FIGURE 7. (a) Vacuum characteristic impedance using a circular signal conductor of a microstrip fixture. (b) The characteristic impedance of RO4003C is inserted in a circular signal conductor microstrip fixture.

can be done by using the following (35),

$$\varepsilon_r^* = 4\frac{h_e}{D}\frac{1}{\exp\left\{\frac{\ln\left(\frac{1}{4}+4\frac{h_e}{D}\right)}{\varepsilon^*_{effR}}\right\} - x} \tag{35}$$

where $x \approx 0.86$. From all corrections made beforehand through (26) and (30), it's defined a new effective complex permittivity substituted to (27) and (33), and becomes as given below,

$$\varepsilon^*_{effR} = \varepsilon'_{eff}\left(1 - j\tan\delta_{eff}\right) \tag{36}$$

The method focuses on wafers from the designed fixture. This new material characterization procedure answers industrial inquiries or needs and researchers by reducing the time and money spent, improving accuracy, and expanding the scanned frequency.

IV. MEASUREMENT SET-UP AND TECHNIQUE VALIDATION

Two microstrip test cells have been designed and manufactured. Both fixtures are identical, with $l_1 = 50$ mm and $l_2 = 70$ mm lengths. The signal conductor is circular with an outer radius $r_0 =$ of 2.5 mm, and the test cell is suitable for changing material thickness. The brass has been used as the ground plan and the signal conductors. Rogers RO4003C, alumina 99.6%, and vinifera have been used to validate the developed process and have a thickness (h) of 1.54 mm, 2.067 mm, and 1.078 mm. To validate the method, the vector network analyzer (VNA) Anritsu MS4642B was utilized as the radiofrequency (RF) measuring analyzer (VNA). In addition, we have investigated the frequency range (0.08–8) GHz. Therefore, three measurements are required: two in the presence of a vacuum, using both test cells, and one with the most extended fixture, which traps the SUT. The measurement

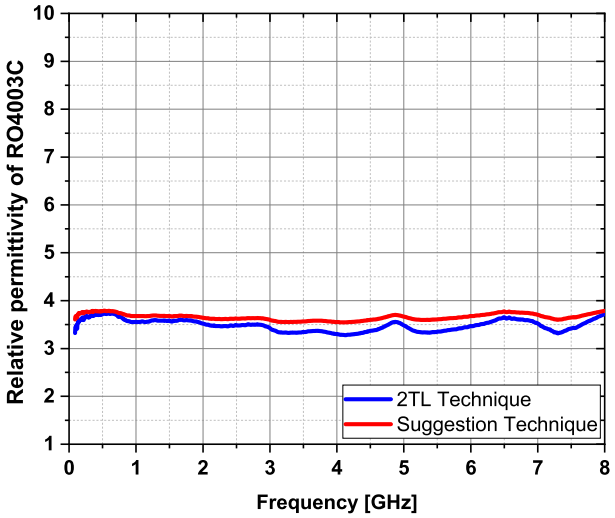

FIGURE 8. The extracted relative permittivity of RO4003C with both techniques.

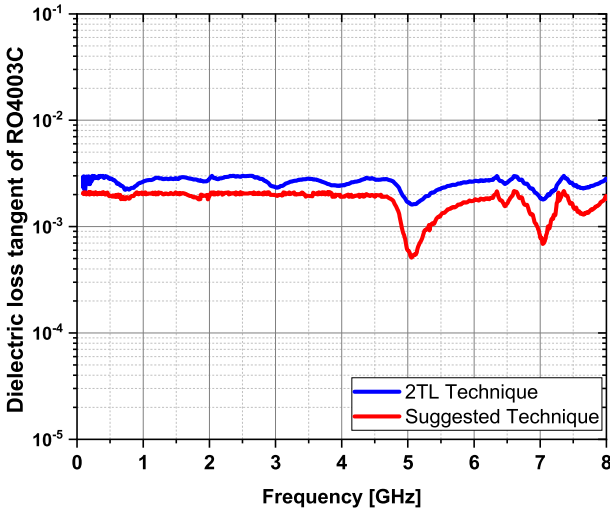

FIGURE 9. The extracted dielectric loss tangent of RO4003C.

fixture is depicted in Figs. 5 and 6. It has been fabricated to experiment with samples and validate the suggested method.

When the SUT is trapped inside the fixture, Fig. 5, becomes as illustrated in Fig. 6.

The measurement apparatus was designed and adapted for hard, soft, and flexible wafers. Liquid, mud, and powder materials might be used with another fixture. The knob controls the material thickness. The 2.067 mm, 1.54 mm, and 1.078 mm are thicknesses of alumina 99.6%, RO4003C, and vinifera, respectively. All samples are 20 mm long and rectangular to fit the apparatus designed to measure simultaneously the sample under test, placed on the extended line and the vacuum case for the shortest line. The microwave test cell holds samples up to 10 mm thick.

The material trapper is designed to ease the measurements and can be made both at the same time.

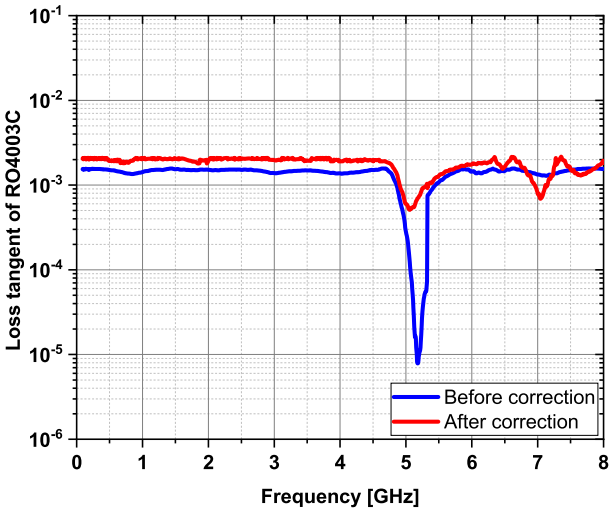

FIGURE 10. Comparison of loss tangent of RO4003C with the new approach.

V. EXPERIMENTAL RESULTS AND DISCUSSION

Below are the results of the characteristic impedances, the relative permittivity, and the loss tangent of the sample material under test.

It observes that the extracted parameters, whose curves are plotted in Fig. 7, don't allow variations to appear brought on by the resonance frequencies. Also, the polynomial function has been to smooth curves, as mentioned in reference [29].

Fig. 8 is derived from the result (35). The new approach's complex effective permittivities are calculated using (36). The correction coefficient is $X \approx 0.846$ when utilizing (18). Its formulation says that it depends on the fixture and the sample material.

At the same time, (32) and (33) are used to determine the effective loss tangent. From the comparison of both expressions, it is well noticed that,

$$\left(1 + \frac{Z_m'' Z_v''}{Z_v' Z_m'}\right) \ll 2 \tag{37}$$

When the dielectric under test is very low-loss. In that case, both extracted loss tangents will differ, as seen in Fig. 9.

Fig. 10 shows the impact of the correction of the effective complex permittivity when using (33).

The method is always compared to the two-line technique, as depicted in Figs. 8-12., which is the most commonly used method. But we set up some particular mechanic processes to reduce their impacts. Hence, the device under test dimensions are well-controlled, especially during the cutting stage. Furthermore, the contact force is a significant parameter to ensure good electrical contact with the sample. This provides reliable measurements for a good study. Under these conditions, the method provides an error of less than 5% on the relative permittivity into the entire frequency range. The following table compares the manufacturer sample intrinsic parameter values and those the new approach got.

As summarized in table 1, the new SUT characterization approach is well-adapted. For example, the median relative

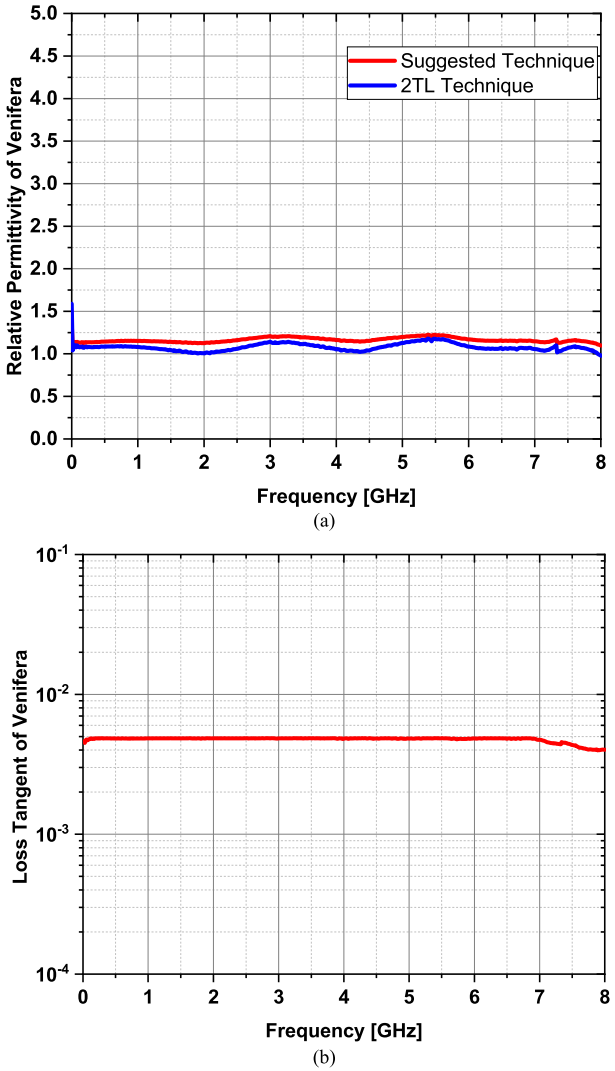

FIGURE 11. (a) The extracted dielectric constant parameter of Vinifera. (b) The extracted dissipation factor parameter of Vinifera.

TABLE 1. Comparison extracted results comparison at 2 GHz.

Designation	Relative permittivity	Loss tangent
Manufacturer	3.55	0.0021
2TL technique	3.519	0.00282
New approach	3.642	0.00194

permittivity values are 3.657 and 3.482 for the suggested method and the two-line technique (using the eigenvalue principle), respectively. In addition, flexible (vinifera) and rigid (alumina 99.6%) wafers have been tested with the same measuring apparatus.

Figs. 11 and 12 are the vinifera and alumina dielectric constant (DK) and dissipation factor (DF) parameters graphs and confirm the suggested method's excellent approach.

Table 2 shows an excellent agreement with those given by the manufacturer; even the method they used hasn't been provided to evaluate the error made.

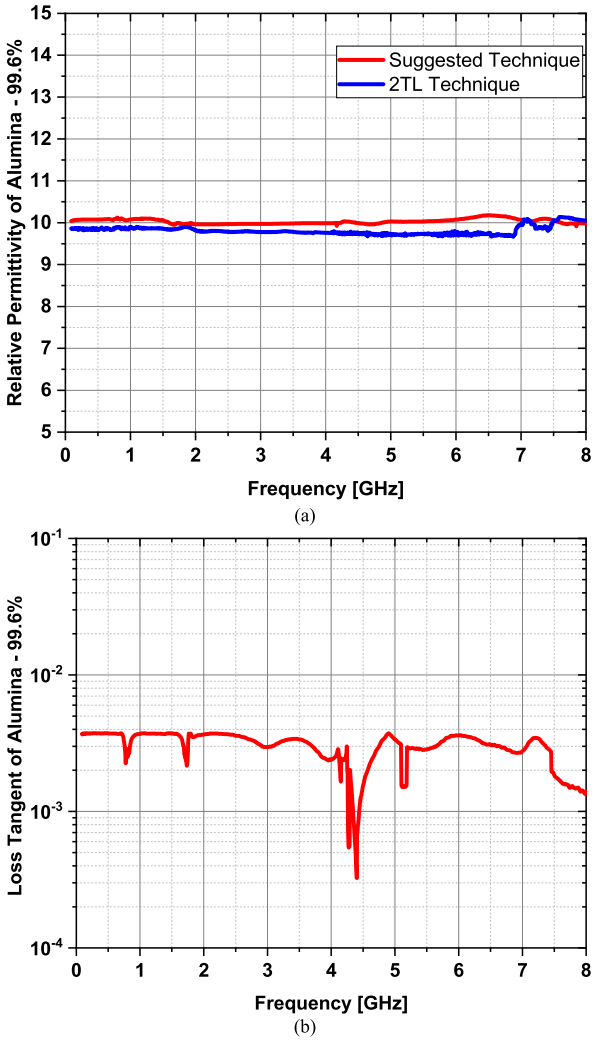

FIGURE 12. (a) The alumina 99.6% extracted dielectric constant parameter. (b) The alumina 99.6% extracted dissipation factor parameter.

TABLE 2. Comparison of the average extracted DK in the frequency range 0.08-8 GHz.

Designation	Alumina 99.6%	RO4003C	Vinifera
Manufacturer	9.3-11.5	3.55	none
Two-line tech.	9.813	3.482	1.079
Suggested Approach	10.031	3.657	1.163

TABLE 3. Comparison of the average extracted DF in the frequency range 0.08-8 GHz.

Designation	Alumina 99.6%	RO4003C	Vinifera
Manufacturer	none	0.0021-0.0027	none
Two-line tech.	0.00351	0.00259	0.00383
Suggested Approach	0.00304	0.00167	0.00476

After using the microstrip measuring test cell depicted in Figs. 5 and 6, and summarizing the DF, illustrated in Figs. 10, 11b, and 12b alongside table 3, the technique has

shown his ability to test material with a minimum DF of 10^{-3} and samples with large and/or small thicknesses in a wide band.

VI. CONCLUSION

We have developed a new approach that combines the propagation constant (without using the eigenvalue principle) and the characteristic impedance to extract the electric intrinsic material properties. In addition, we have investigated how to correct that formula and improved the technique through an automatic coefficient determination. Moreover, we have scanned a large frequency band to validate the principle using three sample materials and compared the results with those proposed by the manufacturer on one side and the two transmission-line (2TL) techniques on the other. This method has the advantage of characterizing simultaneously electric, magnetic, and magneto-electric materials. Moreover, the discontinuity impacts are better solved through this technique.

Furthermore, with fewer measurements (three needed), the semi-filled fixture was enough to experiment with the Rogers RO4003C, alumina 99.6%, and vinifera as available various dielectric materials in our lab., in the frequency range (0.08–8) GHz with error evaluation of less than 5% on the relative permittivity. Finally, the new approach successfully reached the study using the same inhomogeneous frame, and those results were obtained from the two-line technique using the eigenvalue extraction principle. Results from the new approach taught that the order modes, which typically hindered several different technique procedures above a particular frequency, are not a limitation in this new technique. The measuring device is suitable for wafer insulators, and the knob has been set up to control the dielectric under test thickness. One of the advantages of developing this approach is to use magnetic, electric, and magneto-electric materials with the same fixture. There is no need to provide necessarily the material nature and state in advance.

ACKNOWLEDGMENT

The authors sincerely thank the anonymous reviewers for their attentive revision and suggestions to improve the article's quality.

REFERENCES

[1] T. Amadou, M. Balde, F. Manene, and F. Moukanda Mbango, "A dualband bandpass filter with tunable bandwidths for automotive radar and 5G millimeter-wave applications," *Indonesian J. Electr. Eng. Comput. Sci.*, vol. 27, no. 1, pp. 309–317, 2022, doi: 10.11591/ijeecs.v27.i1.pp309-317.

[2] P. Moukala Mpele, F. Moukanda Mbango, D. B. O. Konditi, C. L. Bamy, and F. Urimubenshi, "Compact quadband two-port antenna with metamaterial cell-inspired decoupling parasitic element for mobile wireless applications," *Frequenz*, pp. 1–14, Aug. 2022, doi: 10.1515/freq-2021-0299.

[3] P. Zhang, L. Liu, D. Chen, M. H. Weng, and R. Y. Yang, "Application of a stub-loaded square ring resonator for wideband bandpass filter design," *Electronics*, vol. 9, no. 1, pp. 1–14, 2020, doi: 10.3390/electronics9010176.

[4] T. Liu, Y. Sun, J. Li, J. Yu, and K. Wang, "CPW-fed compact multiband monopole antenna for WLAN/WiMAX/X-band application," *Prog. Electromagn. Res. Lett.*, vol. 87, pp. 105–113, 2019, doi: 10.2528/pierl19080902.

[5] W. Pisula, "Characterization of electronic materials," *Electron. Mater.*, vol. 3, no. 3, pp. 263–264, Oct. 2022, doi: 10.3390/electronicmat3030022.

[6] J. Baker-Jarvis, M. D. Janezic, and D. C. Degroot, "High-frequency dielectric measurements," *IEEE Instrum. Meas. Mag.*, vol. 13, no. 2, pp. 24–31, Apr. 2010, doi: 10.1109/MIM.2010.5438334.

[7] F. Moukanda Mbango, M. G. Lountala, E. J. D. MPemba, F. Ndagijimana, D. Lilonga-Boyenga, and B. MPassi-Mabiala, "Comparison of materials characterization methods using one-port and two-port transmission line principles," *Int. J. Eng. Appl.*, vol. 9, no. 6, pp. 370–381, 2021, doi: 10.15866/irea.v9i6.19679.

[8] D. M. Pozar, *Microwave Engineering*, 4th ed. Hoboken, NJ, USA: Wiley, 2012, doi: 10.4236/jep.2012.34040.

[9] P. López-Rodríguez, D. Escot-Bocanegra, D. Poyatos-Martínez, and F. Weinmann, "Comparison of metal-backed free-space and open-ended coaxial probe techniques for the dielectric characterization of aeronautical composites," *Sensors*, vol. 16, no. 7, pp. 967–981, 2016, doi: 10.3390/s16070967.

[10] F. Moukanda Mbango, A. Al Takach, and F. Ndagijimana, "Complex relative permittivity extraction technique of biotechnology materials in microwaves domain," *Int. J. Electron., Commun. Instrum. Eng. Res. Develop.*, vol. 9, no. 1, pp. 33–42, 2019, doi: 10.24247/ijecierdjun20195.

[11] O. Gbotemi, S. Myllymaki, J. Juuti, M. Teirikangas, H. Jantunen, M. Macek, D. Suvorov, M. Sloma, and M. Jakubowska, "Microwave characterization of printed inductors with ferrimagnetic $BaFe_{12}O_{19}$ composite layers," *IEEE Trans. Magn.*, vol. 53, no. 2, pp. 1–6, Feb. 2017, doi: 10.1109/TMAG.2016.2616468.

[12] E. Lourenço Chuma, Y. Iano, L. L. B. Roger, and G. Fontgalland, "Measuring dielectric properties by two methods using software-defined radio," *IET Sci., Meas. Technol.*, vol. 13, no. 7, pp. 1003–1008, Sep. 2019, doi: 10.1049/iet-smt.2018.5094.

[13] K. Y. You, Z. Abbas, M. F. A. Malek, and E. M. Cheng, "Non-destructive dielectric measurements and calibration for thin materials using waveguide-coaxial adaptors," *Meas. Sci. Rev.*, vol. 14, no. 1, pp. 16–24, 2014, doi: 10.2478/msr-2014-0003.

[14] M. W. Hyde IV, J. W. Stewart, M. J. Havrilla, W. P. Baker, E. J. Rothwell, and D. P. Nyquist, "Nondestructive electromagnetic material characterization using a dual waveguide probe: A full wave solution," *Radio Sci.*, vol. 44, no. 3, pp. 1–13, Jun. 2009, doi: 10.1029/2008rs003937.

[15] J. Baker-Jarvis, "Dielectric characterization of low-loss materials a comparison of techniques," *IEEE Trans. Dielectr. Electr. Insul.*, vol. 5, no. 4, pp. 571–577, Aug. 1998, doi: 10.1109/94.708274.

[16] S. L. S. Severo, Á. A. A. D. Salles, B. Nervis, and B. K. Zanini, "Non-resonant permittivity measurement methods," *J. Microw., Optoelectron. Electromagn. Appl.*, vol. 16, no. 1, pp. 297–311, Mar. 2017, doi: 10.1590/2179-10742017v16i1890.

[17] H. H. Gang, D. Wang, and Z. Wang, "A permittivity measurement method based on back propagation neural network by microwave resonator," *Prog. Electromag. Res. C*, vol. 110, pp. 27–38, 2021, doi: 10.2528/PIERC21010706.

[18] D. Ramos, "Novel electromagnetic characterization methods for new materials and structures in aerospace platforms," *Materials*, vol. 15, no. 15, pp. 1–23, 2022, doi: 10.3390/ma15155128.

[19] O. Saf, H. Erol, and A. Erkin, "A method for material characterization of sealing system elastomers using sound transmission loss measurements," *Polym. Test.*, vol. 111, pp. 107618–107627, 2022, doi: 10.1016/j.polymertesting.2022.107618.

[20] X. Bao, L. Wang, Z. Wang, J. Zhang, M. Zhang, and G. Crupi, "Simple, fast, and accurate broadband complex permittivity characterization algorithm: Methodology and experimental validation from 140 GHz up to 220 GHz," *Electronics*, vol. 11, no. 3, pp. 366–398, 2022, doi: 10.3390/electronics11030366.

[21] M. D. S. Matias and L. A. R. Ramirez, "A comparative review of the main techniques for electromagnetic characterization of materials/uma revisão comparativa das principais técnicas de caracterização eletromagnética de materiais," *Brazilian J. Develop.*, vol. 7, no. 7, pp. 75176–75188, Jul. 2021, doi: 10.34117/bjdv7n7-614.

[22] F. J. F. Gonçalves, A. G. M. Pinto, R. C. Mesquita, E. J. Silva, and A. Brancaccio, "Free-space materials characterization by reflection and transmission measurements using Frequency-by-Frequency and multi-frequency algorithms," *Electronics*, vol. 7, no. 10, pp. 3–6, 2018, doi: 10.3390/electronics7100260.

[23] L. Pometcu, A. Sharaiha, R. Benzerga, R. D. Tamas, and P. Pouliguen, "Method for material characterization in a non-anechoic environment," *Appl. Phys. Lett.*, vol. 108, no. 16, pp. 2–6, 2016, doi: 10.1063/1.4947100.

[24] C. Steiner, "Determination of the dielectric properties of storage materials for exhaust gas aftertreatment using the microwave cavity perturbation method," *Sensors*, vol. 20, no. 21, pp. 1–18, 2020, doi: 10.3390/s20216024.
[25] C. P. L. Rubinger and L. C. Costa, "Building a resonant cavity for the measurement of microwave dielectric permittivity of high loss materials," *Microw. Opt. Technol. Lett.*, vol. 49, no. 7, pp. 1687–1690, 2007, doi: 10.1002/mop.22506.
[26] J.-H. Park and J.-G. Park, "Uncertainty analysis of Q-factor measurement in cavity resonator method by electromagnetic simulation," *Social Netw. Appl. Sci.*, vol. 2, no. 5, pp. 1–6, May 2020, doi: 10.1007/s42452-020-2819-8.
[27] A. Massarini and M. K. Kazimierczuk, "Self-capacitance of inductors," *IEEE Trans. Power Electron.*, vol. 12, no. 4, pp. 671–676, Jul. 1997, doi: 10.1109/63.602562.
[28] A. Gorst, K. Zavyalova, S. Shipilov, V. Yakubov, and A. Mironchev, "Microwave method for measuring electrical properties of the materials," *Appl. Sci.*, vol. 10, no. 24, pp. 1–14, 2020, doi: 10.3390/app10248936.
[29] F. Moukanda Mbango, F. Ndagijimana, and A. L. L. Okana, "Dual coaxial probes in transmission, inserted by dielectric with two different thicknesses to extract the material complex relative permittivity: Discontinuity impacts," *Prog. Electromagn. Res. C*, vol. 110, pp. 67–80, 2021, doi: 10.2528/PIERC21010403.
[30] J. E. D. M'Pemba, G. F. Bouesse, F. Moukanda Mbango, and B. M'Passi-Mabiala, "Probes in transmission with material variable thicknesses to extract the material complex relative permittivity in 1.7–3 GHz," *Meas., Sensors*, vols. 20–21, pp. 1–8, Apr. 2022, doi: 10.1016/j.measen.2022.100369.
[31] J. A. Reynoso-Hernandez, "Unified method for determining the complex propagation constant of reflecting and nonreflecting transmission lines," *IEEE Microw. Wireless Compon. Lett.*, vol. 13, no. 8, pp. 351–353, Aug. 2003, doi: 10.1109/LMWC.2003.815695.
[32] A. A. Takach, F. Moukanda Mbango, F. Ndagijimana, M. Al-Husseini, and J. Jomaah, "Two-line technique for dielectric material characterization with application in 3D-printing filament electrical parameters extraction," *Prog. Electromagn. Res. M*, vol. 85, pp. 195–207, 2019, doi: 10.2528/pierm19071702.
[33] J. Baker-Jarvis, E. J. Vanzura, and W. A. Kissick, "Improved technique for determining complex permittivity with the transmission/reflection method," *IEEE Trans. Microw. Theory Techn.*, vol. 38, no. 8, pp. 1096–1103, Aug. 1990, doi: 10.1109/22.57336.
[34] F. Moukanda Mbango, J. E. D. M'pemba, F. Ndagijimana, and B. M'Passi-Mabiala, "Use of two open-terminated coaxial transmission-lines technique to extract the material relative intrinsic parameters," *IEEE Access*, vol. 8, pp. 138682–138689, 2020, doi: 10.1109/ACCESS.2020.3012431.
[35] M. G. Lountala, F. Moukanda Mbango, F. Ndagijimana, and D. Lilonga-Boyenga, "Movable short-circuit technique to extract the relative permittivity of materials from a coaxial cell," *J. Meas. Eng.*, vol. 7, no. 4, pp. 183–194, Dec. 2019, doi: 10.21595/jme.2019.20925.
[36] A. Ebrahimi, J. Coromina, J. Munoz-Enano, P. Velez, J. Scott, K. Ghorbani, and F. Martin, "Highly sensitive phase-variation dielectric constant sensor based on a capacitively-loaded slow-wave transmission line," *IEEE Trans. Circuits Syst. I, Reg. Papers*, vol. 68, no. 7, pp. 2787–2799, Jul. 2021, doi: 10.1109/TCSI.2021.3074570.
[37] M. D. Janezic and J. A. Jargon, "Complex permittivity determination from propagation constant measurements," *IEEE Microw. Guided Wave Lett.*, vol. 9, no. 2, pp. 76–78, Feb. 1999, doi: 10.1109/75.755052.
[38] F. Moukanda Mbango, M. G. Lountala, F. Ndagijimana, and D. Lilonga-Boyenga, "A partially filled shorted coaxial line technique for material relative permittivity determination," *IETE J. Res.*, vol. 67, pp. 1–11, Mar. 2021, doi: 10.1080/03772063.2021.1902866.
[39] N. K. Tiwari and M. J. Akhtar, "Partially filled substrate integrated waveguide-based microwave technique for broadband dielectric characterization," *IEEE Trans. Instrum. Meas.*, vol. 68, no. 8, pp. 2907–2915, Aug. 2019, doi: 10.1109/TIM.2018.2871807.
[40] U. C. Hasar, G. Buldu, M. Bute, J. J. Barroso, T. Karacali, and M. Ertugrul, "Determination of constitutive parameters of homogeneous metamaterial slabs by a novel calibration-independent method," *AIP Adv.*, vol. 4, no. 10, pp. 1–10, 2014, doi: 10.2528/PIER09062501.
[41] F. Caspers, "RF engineering basic concepts: S-parameters," 2012, *arXiv:1201.2346*.
[42] F. Moukanda Mbango and F. Ndagijimana, "Electric parameter extractions using a broadband technique from coaxial line discontinuities," *Int. J. Sci. Res. Manage.*, vol. 7, no. 5, pp. 248–253, May 2019, doi: 10.18535/ijsrm/v7i5.ec01.

FRANCK MOUKANDA MBANGO received the engineering degree in microwave electronics from Université Mouloud Mammeri, Tizi-Ouzou, Algeria, in 2001, and the M.Sc. and Ph.D. degrees in microwave circuits from Institut National Polytechnique (INP) and Université Joseph Fourier, Grenoble, France, in 2003 and 2008, respectively. From 2009 to 2014, he was involved in several telecommunication industrial projects as a Research and Development Engineer and a Research Assistant Consultant to ALTRAN Technologies at Vallourec and as an Electromagnetic Compatibility (EMC) Engineer to the Scientific and Technical Center for Building (CSTB). He is a CAMES Associate Professor with Université Marien Ngouabi, Brazzaville, Congo. He is a former Senior Lecturer with Pan African University Institute for Basic Sciences Technology and Innovation (PAUISTI), Kenya. His research interests include high-frequency material measurement techniques, microwave electromagnetic circuit modeling for wireless applications, electromagnetic environment impact, test tools for electromagnetic compatibility standards, and microwave antenna designs.

GHISLAIN FRAIDY BOUESSE received the Ph.D. degree in nano and microelectronics from Institut National Polytechnique (INP) de Grenoble, France, in 2005. From 2005 to 2007, he served as a part-time Assistant Professor at INP-Grenoble and a Researcher at Tima Laboratory (CIS Group). In 2007, he joined TIEMPO, a start-up company at Montbonnot St-Martin, Grenoble, France, where he worked as an Integrated Circuit Architect Designer. At the same time, he joined Dolphin Integration as the Deputy Director of Technical Strategy. He is a CAMES Senior Lecturer with Université Marien Ngouabi, Brazzaville, Congo. His research interests include asynchronous design, integrated cryptography, circuits' security, neural circuits, microwave electromagnetic material characterization, and planar antenna designs.

FABIEN NDAGIJIMANA received the Ph.D. degree in microwave and optoelectronics from Institut National Polytechnique de Grenoble (INPG), France, in December 1990. He then joined as an Associate Professor at the Faculty of Electrical Engineering ENSERG, where he teaches microwave techniques and electromagnetic modeling. Since September 1997, he has been with the Université Grenoble Alpes, Grenoble, France, where he is a Full Professor with the Institut Universitaire de Technologie (IUT). His research interests include characterization and electromagnetic modeling of microwave devices for wireless applications, signal integrity in high-speed applications, and test tools for electromagnetic compatibility standards.